Letter

Data-Driven Design of Biselective Templates for Intergrowth Zeolites

Daniel Schwalbe-Koda, Avelino Corma, Yuriy Román-Leshkov, Manuel Moliner, and Rafael Gómez-Bombarelli*

Read Online

ACCESS | Metrics & More | Article Recommendations | Supporting Information

ABSTRACT: Zeolites are inorganic materials with wide industrial applications due to their topological diversity. Tailoring confinement effects in zeolite pores, for instance by crystallizing intergrown frameworks, can improve their catalytic and transport properties, but controlling zeolite crystallization often relies on heuristics. In this work, we use computational simulations and data mining to design organic structure-directing agents (OSDAs) to favor the synthesis of intergrown zeolites. First, we propose design principles to identify OSDAs which are selective toward both end members of the disordered structure. Then, we mine a database of hundreds of thousands of zeolite–OSDA pairs and downselect OSDA candidates to synthesize known intergrowth zeolites such as CHA/AFX, MTT/TON, and BEC/ISV. The computationally designed OSDAs balance phase competition metrics and shape selectivity toward the frameworks, thus bypassing expensive dual-OSDA approaches typically used in the synthesis of intergrowths. Finally, we propose potential OSDAs to obtain hypothesized disordered frameworks such as AEI/SAV. This work may accelerate zeolite discovery through data-driven synthesis optimization and design.
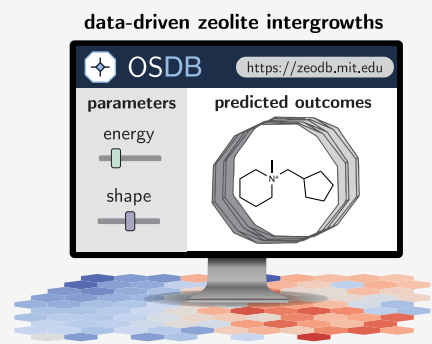
Zeolites are nanoporous materials with a myriad of applications in catalysis and separations.[1,2] Thanks to a broad diversity in topology and composition, their shape selectivity can be tuned along with their thermal stability and catalytic activity.[3] While the complex polymorphism observed in zeolites is key to creating tailored nanoporous materials for targeted applications, it hinders synthesis efforts due to phase competition between different metastable structures. Often, crystallizing a desired framework requires labor-intensive optimization of synthesis conditions to overcome the nucleation and growth of competing phases. Synthesis routes selective toward one framework usually rely on organic structure-directing agents (OSDAs) which template the pore and cage structure of the targeted material.[4] However, selection of cost-effective OSDAs to crystallize the desired frameworks has historically depended on trial-and-error processes.[5] While computational approaches have been developed to design OSDAs *de novo*,[6−9] these methods often lead to complex OSDAs with low synthetic accessibility or low selectivity toward the targeted framework.[10]

Compared to pure-phase frameworks, intergrown zeolites exhibit a structure that is disordered in at least one dimension. Typically, intergrowths are formed by periodic building units related to each other by symmetry operations such as rotations or translations[11] and whose stacking enables them to form a defect-free interface between two topologically distinct domains. Although manually describing such structural faults is possible,[11] computational methods have enabled enumerating intergrown families such as ABC-6[12] or simulating

diffraction patterns.[13] More recently, structural descriptors have been proposed to quantify whether two phases are topologically or geometrically compatible to form intergrown structures.[14]

As differences in local crystallographic environments affect confinement and transport properties, intergrowth zeolites display catalytic behavior distinct from the pure end-member phases.[15,16] For example, the silicoaluminophosphate form of the CHA/AEI intergrowth is a competitive catalyst for the methanol-to-olefin (MTO) reaction compared to the commercial SAPO-34 catalyst.[17,18] However, the challenges of selective zeolite synthesis are exacerbated in the case of intergrowths. Traditional routes for synthesizing the high-silica form of CHA/AEI require the combination of two specific OSDAs for CHA and AEI,[19] which increases the synthesis complexity and cost. In addition, tuning the synthesis conditions to favor the formation of the desired intergrowth requires labor-intensive experimentation. Nevertheless, this dual-OSDA approach has been the standard for crystallizing several intergrown zeolites,[20] despite being limited by (i) the need to design two equally selective OSDAs, (ii) the heuristic

optimization of the synthesis conditions to avoid the collapse to a single phase, and (iii) avoiding formation of extraneous competing phases.

Recently, we have performed high-throughput simulations to quantify phase competition in zeolites.[10,21,22] The large number of simulated zeolite−OSDA pairs allowed rationalizing historical synthesis outcomes from the literature, explaining accessibility windows, and aluminum distributions in single zeolite frameworks as a function of OSDA shape and charge distribution. Furthermore, the data was used to control the synthesis of an aluminosilicate CHA/AEI intergrowth with an OSDA with dual selectivity. By designing OSDAs with shapes and binding energies competitive toward the two frameworks forming the intergrowth, we have demonstrated that this disordered structure can be crystallized in its high-silica form.[10] However, it is unclear whether biselective OSDAs may be designed toward other intergrown frameworks. In this work, we extend the biselectivity design principles toward several other disordered zeolites by combining simulations and data mining. Starting from a data set of hundreds of thousands of zeolite−OSDA pairs, we singled out potential biselective OSDAs for the synthesis of both known and hypothesized intergrowths. To demonstrate the applicability of the method toward small-, medium-, and large-pore zeolites with different cavity sizes, we designed potential biselective OSDAs for the CHA/AFX, MTT/TON, and BEC/ISV intergrowths. Finally, the strategy is extended to several known frameworks and one example of a hypothesized intergrowth. This work is expected to accelerate the discovery of intergrowth zeolites through theory and simulations.

This new computational strategy for designing an intergrowth zeolite is shown in Figure 1. OSDAs known to be selective toward pure-phase zeolites are used as references for the shape, such as *N*-ethyl-*N*-methyl-2,2,6,6-tetramethylpiperidinium for AEI[23] and *N,N,N*-trimethyladamantammonium for CHA[24] (Figure 1a). Then, new OSDAs for the intergrowth can be designed using phase competition and shape metrics. Binding metrics built upon binding energies were calculated for OSDAs retrieved from the literature and for chemically modified ones.[10,25] In particular, we define the competition energy by comparing the binding energies of one OSDA toward all calculated frameworks and adopting the second-best zeolite−OSDA pair as the energy reference. This quantifies how strong the phase competition effects are for a given OSDA, with more negative values indicating less competition. Moreover, the shape of an OSDA is quantified by first projecting the nuclear coordinates of the molecule into a two-dimensional space using a principal component analysis and later measuring the two axes describing the molecule (see Supporting Information).[10] When designing biselective OSDAs for intergrowth systems, we postulate that an ideal biselective OSDA should (i) be an equally strong binder toward both phases forming the intergrowth, (ii) be a weak binder toward all other competing phases (Figure 1b), and (iii) have a geometry that is in-between the reference OSDAs in the shape space, thus favoring the crystallization of both structures (Figure 1c).[10]

Beyond the previously demonstrated CHA/AEI intergrowth, here we discuss the application of this method to many other intergrown zeolites of practical interest. For example, the high-silica CHA/AFX zeolite is used in applications such as the MTO reaction or selective catalytic reduction of NO$_x$ (NO$_x$-SCR) but is typically synthesized using a mixture of OSDAs.[20]
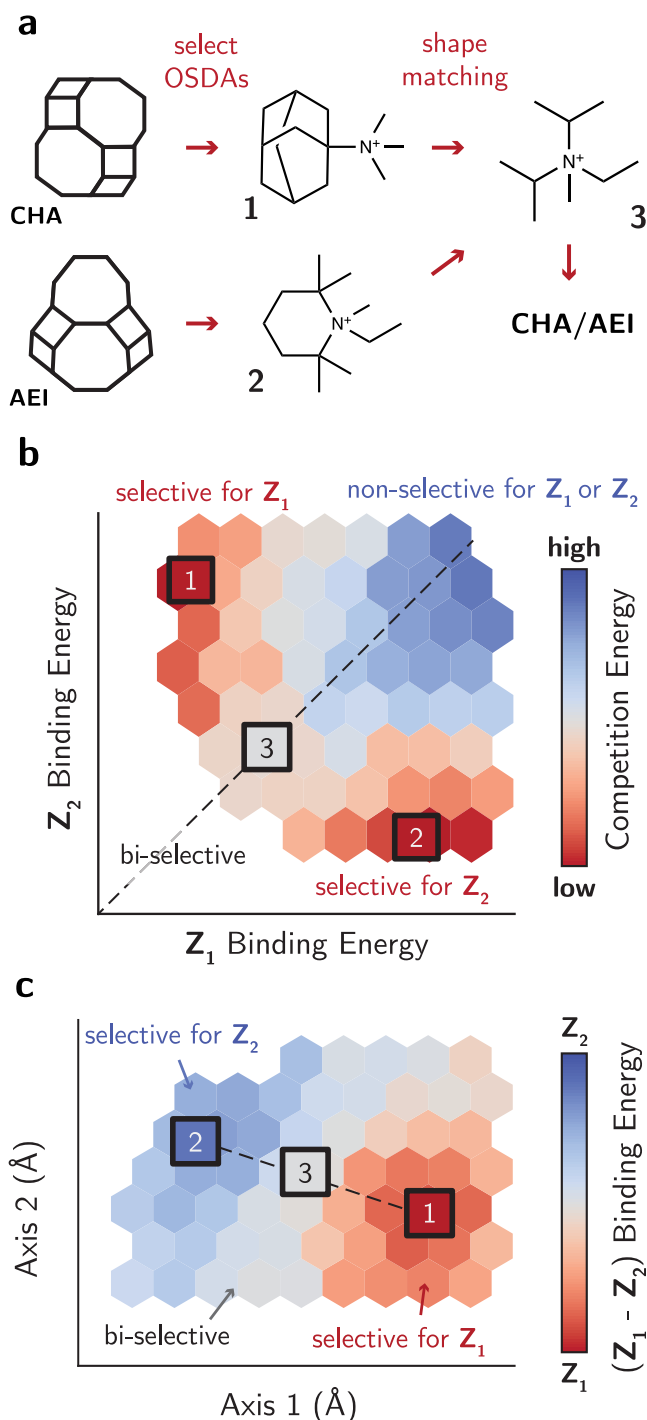
Figure 1. (a) Diagram of the method. Starting from known, selective OSDAs for the synthesis of pure-phase components, a shape interpolation is performed to locate a biselective OSDA. (b) Schematic of predicted OSDA selectivity toward the pure zeolites and the intergrowth. Along with the binding energies, biselective OSDAs should also satisfy (c) shape matching requirements. Often, binding energy metrics give rise to selectivity domains in the shape space.

Although both zeolites are ABC-6 structures and have cages with similar diameters, the *aft* cage in the AFX zeolite is 40% longer than the *cha* cage. This discrepancy in size has led AFX to be synthesized with longer OSDAs, including diquaternary ammonium molecules such as 1,4-bis(1-azoniabicyclo[2.2.2]-
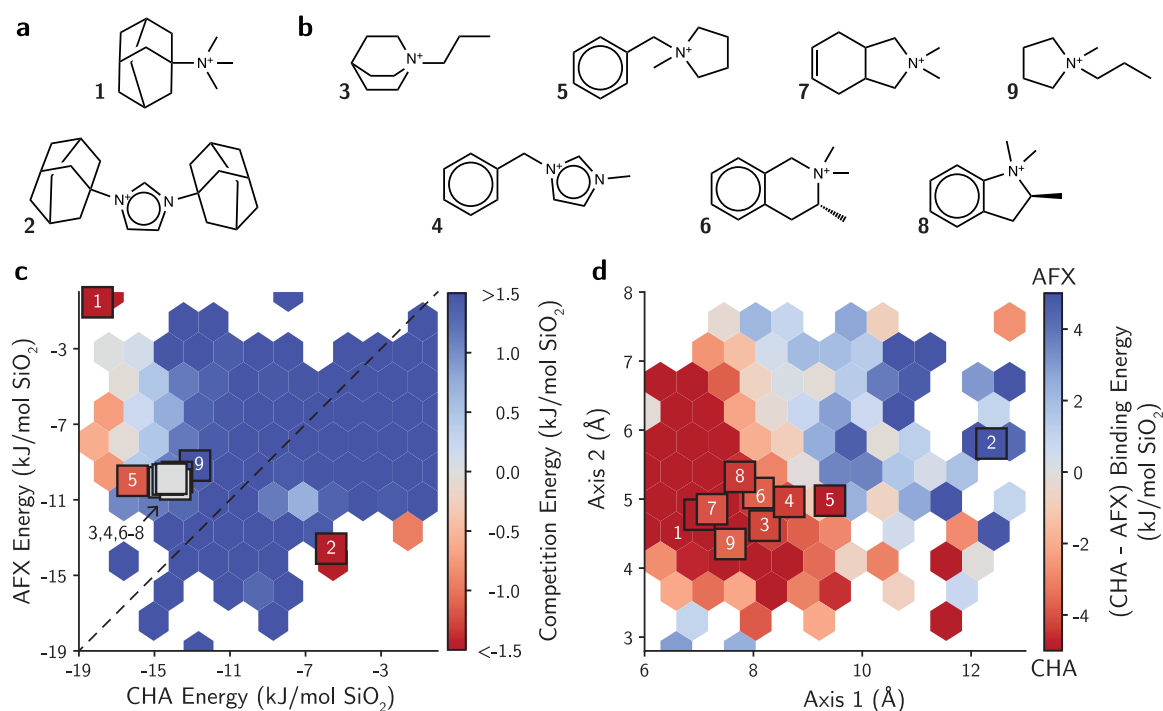
Figure 2. (a) Reference OSDAs for the synthesis of CHA and AFX. (b) Proposed OSDAs for the synthesis of CHA/AFX intergrowth. (c) Phase competition metrics and (d) shape matching between CHA and AFX.
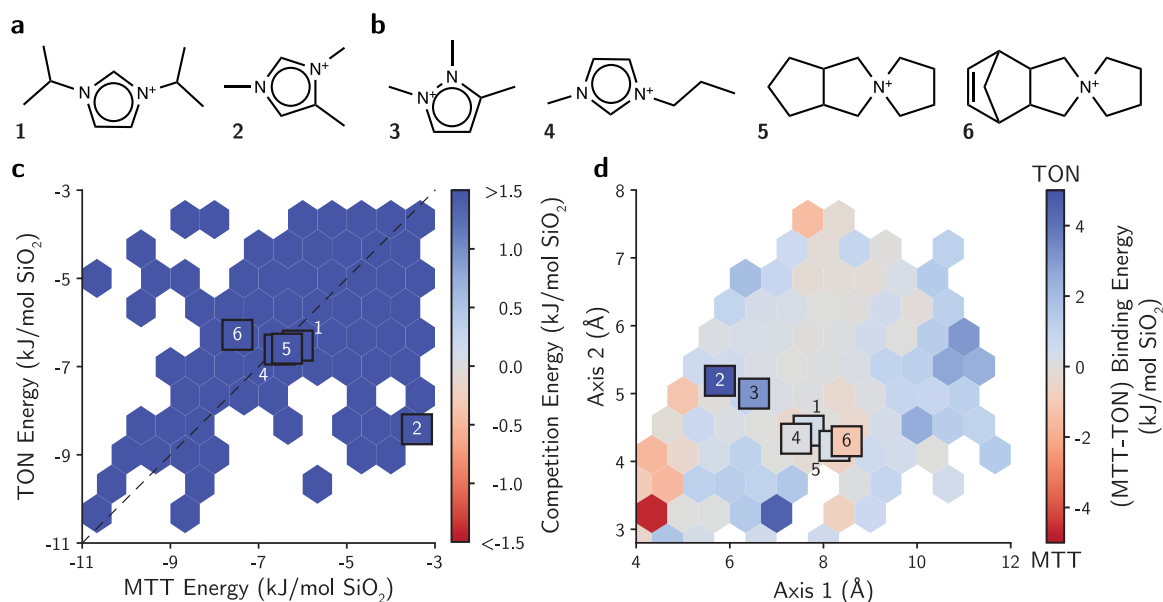

Figure 3. (a) Reference OSDAs for the synthesis of MTT and TON. (b) Proposed OSDAs for the synthesis of MTT/TON intergrowth. (c) Phase competition metrics and (d) shape matching between MTT and TON.

octane)butyl[26] or monocationic OSDAs such as 1,3-bis(1-adamantyl)imidazolium.[27]

Figure 2 shows the proposed OSDAs for a CHA/AFX intergrowth based on the biselectivity design principles. As the *gme* cage in the AFX framework is not occupied by an OSDA but may be stabilized by an inorganic structure-directing agent, the binding energy per SiO_2 alone, as is traditionally normalized, does not determine the likelihood of crystallizing this framework.[10] Quantifying the phase competition effects of both inorganic and organic structure-directing agents at the same could provide additional insights on these phase

boundaries, but simulations with these effects are overly expensive. Instead, the proposed OSDAs can also be compared with respect to their binding energy normalized per OSDA (Table S1 in the Supporting Information), which has been proven useful to describe structure-direction in cage-based zeolites.[10] All computer-designed OSDAs in Figure 2b exhibit intermediate binding energies for both CHA and AFX. In addition, the templates are longer than TMAda, as required to favor the formation of the AFX framework in addition to the *cha* cage. Interestingly, most of the proposed OSDAs may crystallize the *aft* cage by promoting intermolecular $\pi-\pi$
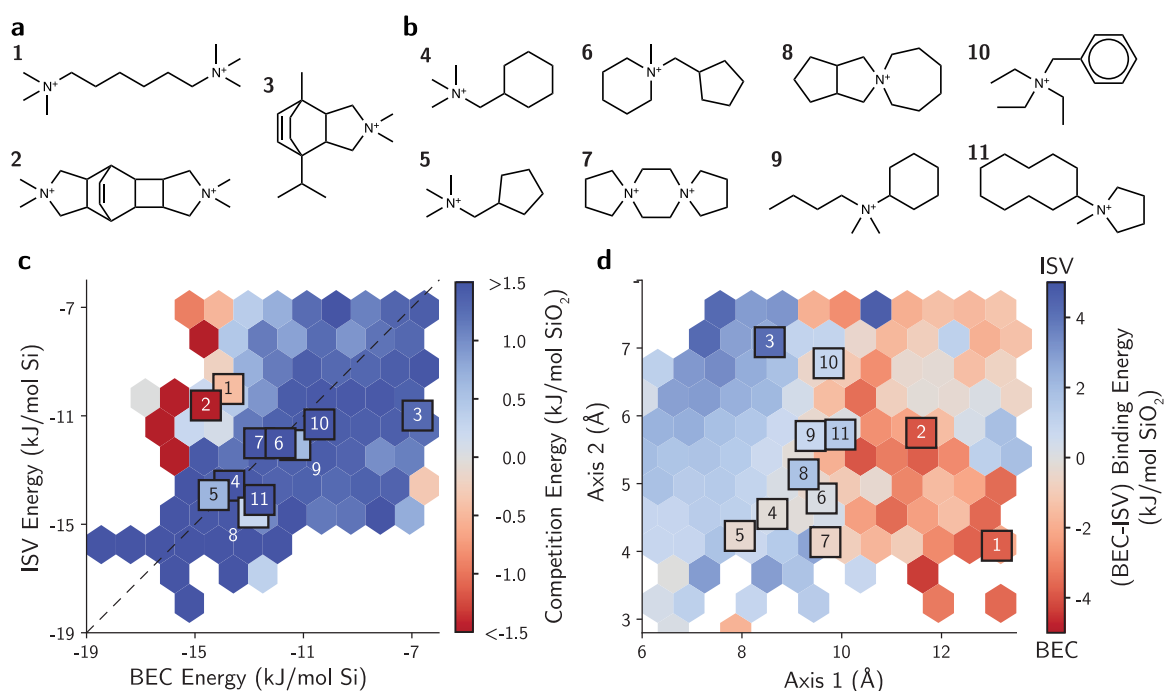
Figure 4. (a) Reference OSDAs for the synthesis of BEC and ISV. (b) Proposed OSDAs for the synthesis of BEC/ISV intergrowth. (c) Phase competition metrics and (d) shape matching between BEC and ISV.

stacking, which enables two molecules to fit in a single *aft* cage (Figure S1 in the Supporting Information). On the other hand, flexible OSDAs may favor the crystallization of the *cha* cage by adopting a folded conformation or the *aft* cage by adopting a stretched conformation (Figure S2).

The MTT and TON zeolites also form intergrowths of practical interest. Both zeolites have one-dimensional medium-sized pores and can be synthesized in the aluminosilicate form. The slight differences in pore sizes of MTT and TON could lead to membranes with high shape selectivity, as has been observed for the MEL/MFI case.[28] However, the synthesis of an MTT/TON intergrowth is typically performed by using the dual-OSDA approach, hindering the control of the phase fraction.[29] Figure 3 shows monocationic OSDAs proposed to enable the control of the MTT/TON intergrowth. Differently from Figure 2a, MTT and TON are not the best possible hosts for most OSDAs based on the phase competition metrics (Figure 3c). However, fine-tuning the synthesis conditions may direct the formation of these zeolites and the corresponding intergrowth. Although synthesis parameters cannot be selected purely through simulations, past literature outcomes and machine learning models trained on them may guide the exploration of synthesis routes.[25,30] Interestingly, since MTT has a slightly smaller unit cell than TON, variations of binding energy with respect to shape depend on the commensurability of the OSDA within the framework (Figure 3d). At a value of 4 Å for Axis 1, OSDAs are more favorable toward MTT than TON. As this value increases, the color shifts toward blue, indicating that slightly longer OSDAs favor TON over MTT. Since the zeolites are simulated with supercells, the pattern starts to repeat at a value of 8 Å for Axis 1. This suggests that an MTT/TON intergrowth could be controlled by varying the length of the molecule, in addition to its binding energy. The examples of OSDAs shown in Figure 3b exhibit a variety of lengths and are likely to direct the formation of the MTT/TON intergrowth.

Finally, we show that the method can also be applied to large-pore, three-dimensional zeolites. One example is the BEC/ISV intergrowth, which is often only obtained in the presence of germanium or fluoride in the synthesis media.[31] Despite the challenge usually associated with predicting OSDAs for zeolites with intersecting pores, the design principles successfully recover the literature results for phase selectivity in BEC and ISV. Figure 4 shows the proposed OSDAs for the synthesis of this intergrown structure. Reference OSDAs for the selective synthesis of BEC are indeed more favorable toward this framework compared to ISV (Figure 4a and c). Furthermore, the red area toward OSDAs with longer Axis 1 in Figure 4d recovers the fact that longer OSDAs favor BEC zeolite, since the unit cells of BEC and ISV have very similar *a* and *b* lattice parameters, but ISV has a *c* lattice parameter 1% smaller than the *c* in the BEC unit cell. Similarly to the MTT/TON example, this indicates that the commensurability between the OSDA and the zeolite is a useful parameter when predicting phase selectivity. From these insights and the results from Figure 4d, we suggest that OSDAs with an Axis 1 between 9 and 10 Å lie in the phase boundary between BEC and ISV and could be used to direct a zeolite intergrowth.

Since this rationale can be extended to any pair of zeolites that are individually templated by OSDAs, biselective OSDAs leading to other intergrown structures can be predicted. In Figures S3−10 in the Supporting Information, we show the applicability of this method toward many other intergrowths, including known disordered structures such as SBS/SBT, FAU/EMT, MEL/MFI, ITH/ITR, RTH/ITE, and ERI/OFF. In cases such as MEL/MFI and RTH/ITE (Figures S3 and 4), the difficulty in distinguishing between phase boundaries may explain why these phases are typically found as intergrowths even when a single OSDA is used. As the shapes of the cavities are very similar, biselectivity is more easily achieved compared to other intergrowths. In other cases such as FAU/EMT, ITH/

ITR, ERI/OFF, and AFS/BPH (Figures S5−8), the shape boundaries are more subtle and often dominated by one of the end members. This suggests that balancing phase competition between the polymorphs could require tuning other synthesis conditions in addition to the OSDA. This is also the case of SBS/SBT (Figure S9), whose intergrowth can be tuned beyond the use of biselective OSDAs by selecting inorganic structure-directing agents that cooperate to crystallize the disordered structure.[32] Finally, OSDAs for realizing the hypothetical intergrowth AEI/SAV (Figure S10) are proposed. Whereas SAV is typically synthesized as a zeotype, synthesizing an aluminosilicate SAV framework intergrown with SSZ-39 (AEI framework) may be interesting for catalytic applications such as NO_x-SCR beyond pure AEI or CHA/AEI intergrowths.

In summary, we combined simulations, data mining, and design principles to propose biselective OSDAs for intergrowth zeolites. By visualizing the OSDAs according to their phase competition and shape matching metrics, we designed promising biselective candidates for cost-efficient synthesis of intergrowth zeolites. The method was demonstrated for small-, medium-, and large-pore zeolites and extended toward several known intergrowths. Furthermore, we proposed OSDAs that could realize a hypothetical intergrowth. This work is expected to accelerate discovery of intergrown zeolites using computation.

■ ASSOCIATED CONTENT

ⓢ Supporting Information

The Supporting Information is available free of charge at https://pubs.acs.org/doi/10.1021/acs.jpclett.1c03132.

> Computational methods, visualizations, and comparisons of binding modes/metrics for proposed OSDAs in CHA/AFX zeolites and proposed OSDAs for eight intergrowth zeolite pairs (PDF)

■ AUTHOR INFORMATION

Corresponding Author

Rafael Gómez-Bombarelli − *Department of Materials Science and Engineering, Massachusetts Institute of Technology, Cambridge, Massachusetts 02139, United States;* ⓞ orcid.org/0000-0002-9495-8599; Email: rafagb@mit.edu

Authors

Daniel Schwalbe-Koda − *Department of Materials Science and Engineering, Massachusetts Institute of Technology, Cambridge, Massachusetts 02139, United States;* ⓞ orcid.org/0000-0001-9176-0854

Avelino Corma − *Instituto de Tecnología Química, Universitat Politécnica de Valéncia-Consejo Superior de Investigaciones Científicas, 46022 Valencia, Spain;* ⓞ orcid.org/0000-0002-2232-3527

Yuriy Román-Leshkov − *Department of Chemical Engineering, Massachusetts Institute of Technology, Cambridge, Massachusetts 02139, United States;* ⓞ orcid.org/0000-0002-0025-4233

Manuel Moliner − *Instituto de Tecnología Química, Universitat Politécnica de Valéncia-Consejo Superior de Investigaciones Científicas, 46022 Valencia, Spain;* ⓞ orcid.org/0000-0002-5440-716X

Complete contact information is available at:

https://pubs.acs.org/10.1021/acs.jpclett.1c03132

■ REFERENCES

(1) Vermeiren, W.; Gilson, J.-P. Impact of Zeolites on the Petroleum and Petrochemical Industry. *Top. Catal.* **2009**, *52*, 1131−1161.

(2) Davis, M. E. Ordered porous materials for emerging applications. *Nature* **2002**, *417*, 813−821.

(3) Li, Y.; Li, L.; Yu, J. Applications of Zeolites in Sustainable Chemistry. *Chem.* **2017**, *3*, 928−949.

(4) Moliner, M.; Rey, F.; Corma, A. Towards the Rational Design of Efficient Organic Structure-Directing Agents for Zeolite Synthesis. *Angew. Chem., Int. Ed.* **2013**, *52*, 13880−13889.

(5) Gallego, E. M.; Portilla, M. T.; Paris, C.; León-Escamilla, A.; Boronat, M.; Moliner, M.; Corma, A. Ab initio" synthesis of zeolites for preestablished catalytic reactions. *Science* **2017**, *355*, 1051−1054.

(6) Lewis, D. W.; Willock, D. J.; Catlow, C. R. A.; Thomas, J. M.; Hutchings, G. J. De novo design of structure-directing agents for the synthesis of microporous solids. *Nature* **1996**, *382*, 604−606.

(7) Sastre, G.; Cantin, A.; Diaz-Cabañas, M. J.; Corma, A. Searching Organic Structure Directing Agents for the Synthesis of Specific Zeolitic Structures: An Experimentally Tested Computational Study. *Chem. Mater.* **2005**, *17*, 545−552.

(8) Pophale, R.; Daeyaert, F.; Deem, M. W. Computational prediction of chemically synthesizable organic structure directing agents for zeolites. *J. Mater. Chem. A* **2013**, *1*, 6750−6760.

(9) Muraoka, K.; Chaikittisilp, W.; Okubo, T. Multi-objective de novo molecular design of organic structure-directing agents for zeolites using nature-inspired ant colony optimization. *Chemical Science* **2020**, *11*, 8214−8223.

(10) Schwalbe-Koda, D.; et al. A priori control of zeolite phase competition and intergrowth with high-throughput simulations. *Science* **2021**, *374*, 308−315.

(11) Baerlocher, Ch; McCusker, L. B. Database of Zeolite Structures. http://www.iza-structure.org/databases/ (accessed 2021-10-25).

(12) Li, Y.; Li, X.; Liu, J.; Duan, F.; Yu, J. In silico prediction and screening of modular crystal structures via a high-throughput genomic approach. *Nat. Commun.* **2015**, *6*, 8328.

(13) Treacy, M. M.; Newsam, J. M.; Deem, M. W. A general recursion method for calculating diffracted intensities from crystals containing planar faults. *Proc. R. Soc. London. Ser. A: Math. Phys. Sci.* **1991**, *433*, 499−520.

(14) Schwalbe-Koda, D.; Jensen, Z.; Olivetti, E.; Gómez-Bombarelli, R. Graph similarity drives zeolite diffusionless transformations and intergrowth. *Nat. Mater.* **2019**, *18*, 1177−1181.

(15) Willhammar, T.; Sun, J.; Wan, W.; Oleynikov, P.; Zhang, D.; Zou, X.; Moliner, M.; Gonzalez, J.; Martínez, C.; Rey, F.; Corma, A. Structure and catalytic properties of the most complex intergrown zeolite ITQ-39 determined by electron crystallography. *Nat. Chem.* **2012**, *4*, 188−194.

(16) Bates, J. S.; Bukowski, B. C.; Harris, J. W.; Greeley, J.; Gounder, R. Distinct Catalytic Reactivity of Sn Substituted in Framework Locations and at Defect Grain Boundaries in Sn-Zeolites. *ACS Catal.* **2019**, *9*, 6146−6168.

(17) Guo, L.; Zhu, W.; Miao, P.; Li, F.; Guo, Z.; Sun, Q. Intergrowth Silicoaluminophosphate Molecular Sieves Synthesized and Their Catalytic Performances for Methanol to Olefins Reaction. *Ind. Eng. Chem. Res.* **2018**, *57*, 10398−10402.

(18) Smith, R. L.; Svelle, S.; del Campo, P.; Fuglerud, T.; Arstad, B.; Lind, A.; Chavan, S.; Attfield, M. P.; Akporiaye, D.; Anderson, M. W. CHA/AEI intergrowth materials as catalysts for the Methanol-to-Olefins process. *Appl. Catal., A* **2015**, *505*, 1−7.

(19) Cao, G.; Mertens, M. M.; Strohmaier, K. G.; Hall, R. B.; Colle, T. H.; Afeworki, M.; Bons, A. J.; Mortier, W. J.; Kliewer, C.; Li, H.; Guram, A. S.; Saxton, R. J.; Muraoka, M. T.; Yoder, J. C. Chabazite-containing molecular sieve, its synthesis and its use in the conversion of oxygenates to olefins. US 7 094 389 B2, 2006.

(20) Naraki, Y.; Ariga, K.; Nakamura, K.; Okushita, K.; Sano, T. ZTS-1 and ZTS-2: Novel intergrowth zeolites with AFX/CHA structure. *Microporous Mesoporous Mater.* **2017**, *254*, 160−169.

(21) Schwalbe-Koda, D.; Gomez-Bombarelli, R. Supramolecular Recognition in Crystalline Nanocavities Through Monte Carlo and Voronoi Network Algorithms. *J. Phys. Chem. C* **2021**, *125*, 3009−3017.

(22) Schwalbe-Koda, D.; Gomez-Bombarelli, R. Benchmarking binding energy calculations for organic structure-directing agents in pure-silica zeolites. *J. Chem. Phys.* **2021**, *154*, 174109.

(23) Schmidt, J. E.; Deem, M. W.; Lew, C.; Davis, T. M. Computationally-Guided Synthesis of the 8-Ring Zeolite AEI. *Top. Catal.* **2015**, *58*, 410−415.

(24) Zones, S. I. Conversion of faujasites to high-silica chabazite SSZ-13 in the presence of N,N,N-trimethyl-1-adamantammonium iodide. *J. Chem. Soc., Faraday Trans.* **1991**, *87*, 3709−3716.

(25) Jensen, Z.; Kwon, S.; Schwalbe-Koda, D.; Paris, C.; Gómez-Bombarelli, R.; Román-Leshkov, Y.; Corma, A.; Moliner, M.; Olivetti, E. A. Discovering Relationships between OSDAs and Zeolites through Data Mining and Generative Neural Networks. *ACS Cent. Sci.* **2021**, *7*, 858−867.

(26) Zones, S. Zeolite SSZ-13 and its method of preparation. US 4 544 538, 1985.

(27) Archer, R. H.; Zones, S. I.; Davis, M. E. Imidazolium structure directing agents in zeolite synthesis: Exploring guest/host relation-ships in the synthesis of SSZ-70. *Microporous Mesoporous Mater.* **2010**, *130*, 255−265.

(28) Kumar, P.; Kim, D. W.; Rangnekar, N.; Xu, H.; Fetisov, E. O.; Ghosh, S.; Zhang, H.; Xiao, Q.; Shete, M.; Siepmann, J. I.; Dumitrica, T.; McCool, B.; Tsapatsis, M.; Mkhoyan, K. A. One-dimensional intergrowths in two-dimensional zeolite nanosheets and their effect on ultra-selective transport. *Nat. Mater.* **2020**, *19*, 443−449.

(29) Wang, B.; Tian, Z.; Li, P.; Wang, L.; Xu, Y.; Qu, W.; Ma, H.; Xu, Z.; Lin, L. Synthesis of ZSM-23/ZSM-22 intergrowth zeolite with a novel dual-template strategy. *Mater. Res. Bull.* **2009**, *44*, 2258−2261.

(30) Jensen, Z.; Kim, E.; Kwon, S.; Gani, T. Z. H.; Román-Leshkov, Y.; Moliner, M.; Corma, A.; Olivetti, E. A Machine Learning Approach to Zeolite Synthesis Enabled by Automatic Literature Data Extraction. *ACS Cent. Sci.* **2019**, *5*, 892−899.

(31) Villaescusa, L. A.; Díaz, I.; Barrett, P. A.; Nair, S.; LLoris-Cormano, J. M.; Martínez-Mañez, R.; Tsapatsis, M.; Liu, Z.; Terasaki, O.; Camblor, M. A. Pure Silica Large Pore Zeolite ITQ-7: Synthetic Strategies, Structure-Directing Effects, and Control and Nature of Structural Disorder. *Chem. Mater.* **2007**, *19*, 1601−1612.

(32) Lee, H.; Shin, J.; Lee, K.; Choi, H. J.; Mayoral, A.; Kang, N. Y.; Hong, S. B. Synthesis of thermally stable SBT and SBS/SBT intergrowth zeolites. *Science* **2021**, *373*, 104−107.